2015 IEEE International Conference on Robotics and Automation (ICRA)
Washington State Convention Center
Seattle, Washington, May 26-30, 2015

Modifying the Kinematic Structure of an Anthropomorphic Arm to Improve Fault Tolerance

K. M. Ben-Gharbia[+], A. A. Maciejewski[+], and R. G. Roberts[*]

***Abstract*— It is well known that anthropomorphic manipulators, such as the PA-10, are intolerant to a single locked joint failure of the elbow. This is because the elbow is the only joint that can change the distance between the spherical shoulder joint and the spherical wrist. In this work, it is shown how such arms can be made significantly more fault tolerant by a minor modification to the kinematic structure of the arm. We quantify the degree of fault tolerance to locked joint failures as the minimum of the smallest singular value of the resulting seven Jacobians over all possible single failures. The DH parameters for the modified arm are designed so that the corresponding fault tolerant properties are close to those of a robot with an optimally failure tolerant Jacobian. The fault tolerance of the designed robot is evaluated for two different classes of applications, i.e., point-to-point motions and specified end-effector trajectories.**

***Index Terms*— redundant robots, robot kinematics, fault-tolerant robots.**

I. Introduction

The design and control of robotic manipulators that can operate after component failures is critical for applications in remote and/or hazardous environments where repair is not possible. One recent example is the Fukushima nuclear reactor accident [1], [2]. The failure rates for components in such harsh environments are relatively high [3], [4]. Many of these component failures will result in a robot's joint becoming immobilized, i.e., a locked joint failure mode, or are frequently transformed into the locked joint failure mode by failure recovery mechanisms that employ fail safe brakes [5]. Because of the severe consequences of such failures there has been a great deal of research to increase manipulator reliability [6], as well as improve failure detection and recovery [7]–[9].

In addition to increasing reliability, another frequently used approach for implementing fault tolerance is to employ kinematically redundant manipulators [10]–[13]. In previous work [14], [15], the focus has frequently been on determining the kinematic design of a robot from the local fault tolerant properties of a desired Jacobian. It is also possible to consider the dynamic properties of the robot as discussed in [16]. In this work we start with the kinematics of a commonly used redundant robot, i.e., an anthropomorphic design like the PA-10, and try to improve its failure tolerant properties.

The remainder of this paper is organized in the following manner. A local definition of failure tolerance centered on desirable properties of the manipulator Jacobian is mathematically defined in the next section. In Section III we describe how one can modify an anthropomorphic arm and design its DH parameters to optimize its degree of fault tolerance. The evaluation of this arm for applications in two different categories of motion are then presented in Section IV. Finally the conclusions of this work are presented in Section V.

II. Background on Optimally Fault-Tolerant Jacobians

In this section we briefly review our definition of an optimally fault tolerant Jacobian [15]. The dexterity of manipulators is frequently quantified in terms of the properties of the manipulator Jacobian matrix, which relates end-effector velocities to joint angle velocities. The Jacobian will be denoted by the $m \times n$ matrix J where m is the dimension of the task space and n is the number of degrees of freedom of the manipulator. For redundant manipulators, $n > m$ and the quantity $n-m$ is the degree of redundancy. The manipulator Jacobian can be written as a collection of columns

$$J_{m\times n} = \begin{bmatrix} j_1 & j_2 & \cdots & j_n \end{bmatrix} \tag{1}$$

where j_i represents the end-effector velocity due to the velocity of joint i. For an arbitrary single joint failure at joint f, assuming that the failed joint can be locked, the resulting m by $n-1$ Jacobian will be missing the fth column, where f can range from 1 to n. This Jacobian will be denoted by a preceding superscript so that in general

$${}^{f}J_{m\times(n-1)} = \begin{bmatrix} j_1 & j_2 & \cdots & j_{f-1} & j_{f+1} & \cdots & j_n \end{bmatrix}. \tag{2}$$

The properties of a manipulator Jacobian are frequently quantified in terms of the singular values, denoted σ_i, which are typically ordered so that $\sigma_1 \geq \sigma_2 \geq \cdots \geq \sigma_m \geq 0$. The most significant of the singular values is σ_m, the minimum singular value, because it is a measure of the worst-case dexterity over all possible end-effector motions.

The definition of failure tolerance used in this work is based on the worst-case dexterity following an arbitrary single locked joint failure. Because ${}^{f}\sigma_m$ denotes the minimum singular value of ${}^{f}J$, ${}^{f}\sigma_m$ is a measure of the worst-case dexterity if joint f fails. If all joints are equally likely to

This work was supported in part by the National Science Foundation under Contract IIS-0812437.

This research utilized the CSU ISTeC Cray HPC System supported by NSF Grant CNS-0923386.

[+]K. M. Ben-Gharbia and A. A. Maciejewski are with the Department of Electrical and Computer Engineering, Colorado State University, Fort Collins, CO 80523-1373 USA {khaled.ben-gharbia, aam}@colostate.edu

[*]R. G. Roberts is with the Department of Electrical and Computer Engineering, Florida A&M–Florida State University, Tallahassee, FL 32310-6046 USA rroberts@eng.fsu.edu

TABLE I: The DH parameters of PA–10 robot

i	α_i [degrees]	a_i [m]	d_i [m]	θ_i [degrees]
1	-90	0	0	θ_1
2	90	0	0	θ_2
3	-90	0	0.450	θ_3
4	90	0	0	θ_4
5	-90	0	0.5	θ_5
6	90	0	0	θ_6
7	0	0	0.08	θ_7

fail, then a measure of the worst-case failure tolerance is given by

$$\mathcal{K} = \min_{f=1}^{n}({}^{f}\sigma_m). \tag{3}$$

To insure that manipulator performance is optimal prior to a failure, an optimally failure tolerant Jacobian is further defined as having all equal singular values due to the desirable properties of isotropic manipulator configurations. Under these conditions, one can show that $\mathcal{K}$ is governed by the inequality

$$\mathcal{K} = \min_{f=1}^{n}({}^{f}\sigma_m) \leq \sigma\sqrt{\frac{n-m}{n}} \tag{4}$$

where σ denotes the norm of the original Jacobian.

For the case of a seven degree-of-freedom manipulator operating in a six dimensional task space, one example of a Jacobian that is very close to an optimally failure tolerant configuration is given by [19]:

$$J = \begin{bmatrix} 1 & 0.43 & 0.75 & -0.54 & 0.14 & 0.33 & -0.38 \\ 0 & -0.60 & 0.65 & 0.46 & -0.79 & -0.19 & -0.81 \\ 0 & -0.67 & -0.14 & -0.70 & 0.60 & -0.93 & -0.46 \\ 0 & 0.77 & 0.15 & 0.84 & 0.58 & -0.69 & -0.43 \\ 1 & -0.15 & -0.36 & 0.33 & -0.42 & -0.72 & 0.59 \\ 0 & 0.62 & -0.92 & -0.43 & -0.69 & -0.10 & -0.68 \end{bmatrix}, \tag{5}$$

where $\mathcal{K} = 0.5196$, and its singular values range between $\sigma_1 = 1.5829$ and $\sigma_m = \sigma_6 = 1.4726$, i.e., nearly isotropic. In the next section, we will discuss how one can modify an anthropomorphic arm to be close to the degree of fault tolerance exhibited by this Jacobian.

III. Modifying the Anthropomorphic Arm Design

It is interesting to note that robots with a kinematic design that is similar to a seven degree-of-freedom human arm, e.g., the Mitsubishi PA–10 (the DH parameters are presented in Table I), are very fault intolerant. This is because the fourth joint, i.e., the elbow, is critical as it is the only joint that can change the distance from the spherical shoulder to the spherical wrist. Thus if the robot's tool is close to the wrist, the wrist joints cannot significantly compensate for a loss in linear velocity due to motion of the elbow. One way to mitigate this issue, and improve the fault tolerance to a failure in the elbow joint, is to use a bigger tool offset. However, this will still not achieve the optimal fault tolerance of the designs discussed here.

Another alternative is to physically modify the design of an anthropomorphic arm structure by moving the third joint

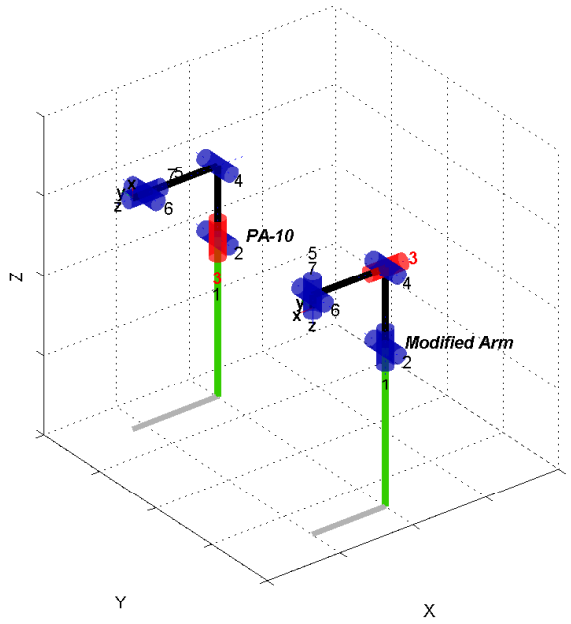

Fig. 1: Modifying the PA-10 to be fault tolerant. Note that the third joint is moved from the base frame to the same location as the coordinate frame of the fourth joint. This is a result of considering the joint offsets d_3 and d_5 to be link lengths a_2 and a_4. To help with visualizing this difference, the joint values for the PA-10 are set to $[\,0^\circ\,,\,0^\circ\,,\,0^\circ\,,\,-90^\circ\,,\,0^\circ\,,\,0^\circ\,,\,0^\circ]$, whereas for the modified arm the joint values are $[\,0^\circ\,,\,-90^\circ\,,\,0^\circ\,,\,-90^\circ\,,\,0^\circ\,,\,0^\circ\,,\,0^\circ]$. (This graphic was generated using the Robotics Toolbox described in [17].)

to be together with the fourth joint at the same coordinate frame. Table II presents the resulting DH parameters, where the parameters a_2, a_4, and d_7 can be designed to further optimize fault tolerance. Note that moving the third joint in this way interchanged the roles of the d offsets and the a link lengths for some of the joints. However, the robots still share similar physical structure as indicated in Fig. 1.

In this work we chose the Jacobian in (5) for comparison with the modified anthropomorphic arm. In order to obtain a fair comparison with (5), we chose the values of a_2, a_4, and d_7 so that the average of the singular values

$$\sigma_{ave} = \frac{1}{6}\sum_{i=1}^{6}\sigma_i \tag{6}$$

is close to the average of the singular values of (5). To do this, we first randomly generated one million uniformly distributed points in the joint space. We chose $a_2 = a_4 = a$ as an approximation to the lengths of a human arm, and varied a to be 1, 2, and 3. We then varied d_7 to be in the range of 0 to 100% of a, in 10% increments. Note that when identifying the fault tolerance of a manipulator Jacobian, one should remember that scaling the length parameters essentially changes the weighting between the position and orientation. Otherwise, it might be tempting to think that two

TABLE II: Kinematics of a modified anthropomorphic arm

i	α_i [degrees]	a_i [m]	d_i [m]	θ_i [degrees]
1	-90	0	0	θ_1
2	90	a_2	0	θ_2
3	-90	0	0	θ_3
4	90	a_4	0	θ_4
5	-90	0	0	θ_5
6	90	0	0	θ_6
7	0	0	d_7	θ_7

(a_2, a_4, d_7) combinations that are proportional to each other would result in the same fault tolerance properties. Thus each of the above 33 selections will generally result in different fault tolerance properties. For each of the 33 resulting robots, we calculated one million Jacobians corresponding to the one million configurations generated earlier, and evaluated (6). The robot parameters that resulted in a configuration that most closely matched the average singular value of the nominal Jacobian in (5) were $a = 2$ and $d_7 = 1$.

A desirable configuration should have a large $\mathcal{K}$ value and should be close to being isotropic. In the next step we optimized the joint configuration and d_7 value in terms of both $\mathcal{K}$ and the isotropy measure

$$\mathcal{I} = \frac{\sigma_6}{\sigma_1}. \tag{7}$$

Note that $\mathcal{I}$ is the reciprocal of the condition number and is well defined for any nonzero matrix. Unlike the condition number, $\mathcal{I}$ is bounded and takes on the optimal value 1 when the configuration is isotropic and the value 0 at a singularity. In general, larger values of $\mathcal{I}$ correspond to better configurations in the sense of isotropy. In order to take into account both measures, we chose to maximize $\rho \cdot \mathcal{K} + \mathcal{I}$, where ρ is a user specified parameter to set the relative importance of optimizing $\mathcal{K}$ versus $\mathcal{I}$. (In this work we selected $\rho = 1$ to consider them both equally.) This was accomplished using a nullspace projection method. For each of the one million starting configurations, we used the projection of the gradient of $\rho \cdot \mathcal{K} + \mathcal{I}$ onto the nullspace to determine the joint motion that would improve fault tolerance and isotropy:

$$\dot{\theta} = (I - J^+ J)\left(\rho \cdot \nabla\mathcal{K} + \nabla\mathcal{I}\right). \tag{8}$$

Applying (8) reconfigures the robot along its self-motion manifold to a maximum value for $\rho \cdot \mathcal{K} + \mathcal{I}$ subject to the constraint of not moving the end effector.[1] The gradients for $\mathcal{K}$ and $\mathcal{I}$ are found using the method described in [3]. In [3] it was noted that $\mathcal{K}$ can be written as

$$\mathcal{K} = {}^F u_6^T \; {}^F J \; {}^F v_6 \tag{9}$$

where $F = \arg\min_{f=1,\ldots,7} {}^f\sigma_6$ is the index of the most debilitating joint failure and ${}^F u_6$ and ${}^F v_6$ are respectively the input and output singular vectors corresponding to the minimum singular value of ${}^F J$. The gradient of $\mathcal{K}$ is found by taking its partial derivatives, which results in three terms.

[1] In practice, a position error term is required to make sure that the end effector is not moved [18].

It is not difficult to show that the first and third terms are zero, i.e.,

$$\left(\frac{\partial \; {}^F u_6^T}{\partial \theta_i}\right) {}^F J \; {}^F v_6 = {}^F u_6^T \; {}^F J \left(\frac{\partial \; {}^F v_6}{\partial \theta_i}\right) = 0 \tag{10}$$

because the partial derivatives of ${}^F u_6^T \; {}^F u_6 = {}^F v_6^T \; {}^F v_6 = 1$ are zero. Thus, we have that the partial derivative of $\mathcal{K}$ is given by

$$\frac{\partial \mathcal{K}}{\partial \theta_i} = {}^F u_6^T \left(\frac{\partial \; {}^F J}{\partial \theta_i}\right) {}^F v_6. \tag{11}$$

To obtain the partial derivative of ${}^F J$ with respect to θ_i, we use the fact that for rotary-jointed robots

$$\frac{\partial j_k}{\partial \theta_i} = \begin{cases} \begin{bmatrix} (z_i \times z_k) \times p_k + z_k \times (z_i \times p_k) \\ z_i \times z_k \end{bmatrix} & i < k \\ \begin{bmatrix} z_k \times (z_i \times p_k) \\ 0 \end{bmatrix} & i \geq k \end{cases} \tag{12}$$

where z_l is the axis of rotation of the l-th joint and p_l is the vector from the l-th joint axis to the end effector. The expression for $\partial j_k / \partial \theta_i$ can be simplified to

$$\frac{\partial j_k}{\partial \theta_i} = \begin{cases} \begin{bmatrix} (z_i^T p_k) z_k - (z_i^T z_k) p_k \\ z_i \times z_k \end{bmatrix} & i < k \\ \begin{bmatrix} (z_k^T p_i) z_i - (z_i^T z_k) p_i \\ 0 \end{bmatrix} & i \geq k. \end{cases} \tag{13}$$

The gradient of $\mathcal{K}$,

$$\nabla\mathcal{K} = \begin{bmatrix} \frac{\partial \mathcal{K}}{\partial \theta_1} & \frac{\partial \mathcal{K}}{\partial \theta_2} & \cdots & \frac{\partial \mathcal{K}}{\partial \theta_7} \end{bmatrix}^T, \tag{14}$$

is then given by using (11) and (13).

The gradient of $\mathcal{I}$,

$$\nabla\mathcal{I} = \begin{bmatrix} \frac{\partial \mathcal{I}}{\partial \theta_1} & \frac{\partial \mathcal{I}}{\partial \theta_2} & \cdots & \frac{\partial \mathcal{I}}{\partial \theta_7} \end{bmatrix}^T, \tag{15}$$

is found in an analogous manner by taking the partial derivatives of

$$\mathcal{I} = \frac{\sigma_6}{\sigma_1} = \frac{u_6^T J v_6}{u_1^T J v_1}, \tag{16}$$

to obtain

$$\frac{\partial \mathcal{I}}{\partial \theta_i} = \frac{\sigma_1 \left(u_6^T \frac{\partial J}{\partial \theta_i} v_6\right) - \sigma_6 \left(u_1^T \frac{\partial J}{\partial \theta_i} v_1\right)}{\sigma_1^2} \tag{17}$$

where $\partial J / \partial \theta_i$ is given column wise by (13) and u_i and v_i are the ith output and input singular vectors of J, respectively.

We then evaluated 21 robots with $a_2 = a_4 = a = 2$ and varying d_7 from 0 to $a = 2$ in increments of 0.1 by starting with the original one million randomly generated configurations and using the above approach to drive the robot to a configuration that maximized $\rho \cdot \mathcal{K} + \mathcal{I}$. We then selected the optimal joint configuration to be the one that corresponds to the maximum value of $\mathcal{K} = 0.3672$, which resulted in

$$\theta = [0^\circ \; 23^\circ \; 132^\circ \; 316^\circ \; 307^\circ \; 273^\circ \; 114^\circ]^T, \tag{18}$$

and $d_7 = 1.1$. Fig. 2 illustrates an image of the robot at the optimized configuration and its DH parameters are given in Table III.

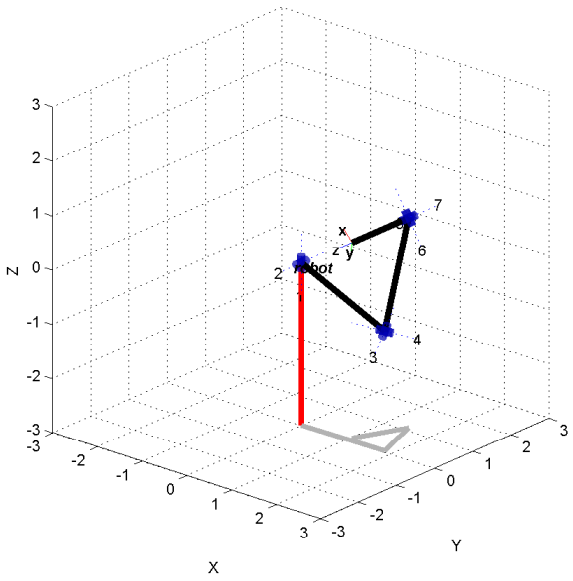

Fig. 2: The locally optimal fault tolerant configuration at the design point of the modified anthropomorphic arm. (This graphic was generated using the Robotics Toolbox described in [17].)

TABLE III: Modified anthropomorphic arm with optimized DH parameters

i	α_i [degrees]	a_i [m]	d_i [m]	θ_i [degrees]
1	-90	0	0	0°
2	90	2	0	23°
3	-90	0	0	132°
4	90	2	0	316°
5	-90	0	0	307°
6	90	0	0	273°
7	0	0	1.1	114°

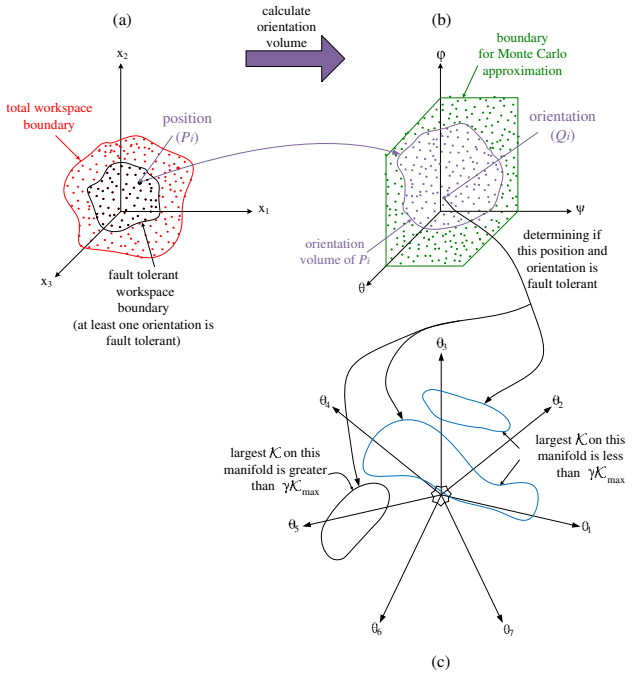

Fig. 3: An illustration of how Monte Carlo integration is used to compute the six-dimensional volumes of both the fault-tolerant workspace and the reachable workspace. For each reachable workspace position P_i in (a) we use Monte Carlo integration to evaluate the achievable orientation volume at that P_i as shown in (b). To evaluate the fault tolerance of a P_i and Q_i in (b) one needs to identify if the maximum value of $\mathcal{K} \geq \gamma \mathcal{K}_{\max}$ for all self-motion manifolds associated with that P_i and Q_i, as shown in (c), where $0 \geq \gamma \leq 1$ is a user defined parameter, and $\mathcal{K}_{\max}$ is the $\mathcal{K}$ value of (5). The three-dimensional fault-tolerant volume contains all of the positions that have at least one fault-tolerant orientation.

IV. Results

A. Fault Tolerant Workspace Identification

At this step we have designed our arm to be fault tolerant at one particular configuration. To evaluate the total workspace one can use the algorithm in [19] to calculate the three- and six-dimensional workspaces. Fig. 3 illustrates the algorithm where one needs to evaluate the maximum of $\mathcal{K}$ at every point, i.e., a position and an orientation, and each position has associated with it its own orientation volume [19]. (In this work, a point is chosen to be fault tolerant if its maximum $\mathcal{K} > 0.2$). However, there are typically multiple self-motion manifolds [15] at every point. The question of whether one should allow configurations that represent maximum $\mathcal{K}$ values to switch between disjoint manifolds depends on the application, e.g., it may be appropriate for pick and place applications but not for those requiring a specified trajectory for the end effector.

B. Fault Tolerant Point-to-Point Motion

Examples for three trajectories are chosen to measure the variation of maximum $\mathcal{K}$ as the robot moves away from the design point, when allowing the searching through all possible self-motion manifolds associated with a point to find the maximum $\mathcal{K}$. Fig. 4 illustrates the maximum value of $\mathcal{K}$ for trajectories along the x-axis, y-axis, and z-axis that cross the design point, with the orientation held constant. One can note that the design point is still the best in terms of fault tolerance, which corresponds to the joint configuration solution that was calculated in Section III. In order to always maintain maximum $\mathcal{K}$, the magnitude of joint change will vary significantly at some positions in the trajectories as a result of allowing the jump to different self-motion manifolds. This is acceptable for pick and place tasks.

The total three-dimensional volume is at its maximum value, i.e., a sphere with a volume of $\frac{4}{3}\pi R_{max}^3$, where the maximum reach $R_{max} = 5.1$ m. The total six-dimensional workspace is 49% of the maximum six-dimensional volume, i.e., $\frac{4}{3}\pi R_{max}^3 \cdot \pi^2$ [19]. Fig. 5 illustrates the total six-dimensional workspace, where the three-dimensional volume part is shown with multiple cross-sections at the design point to better visualize the interior. The color map represents the orientation volume distribution within the three-dimensional

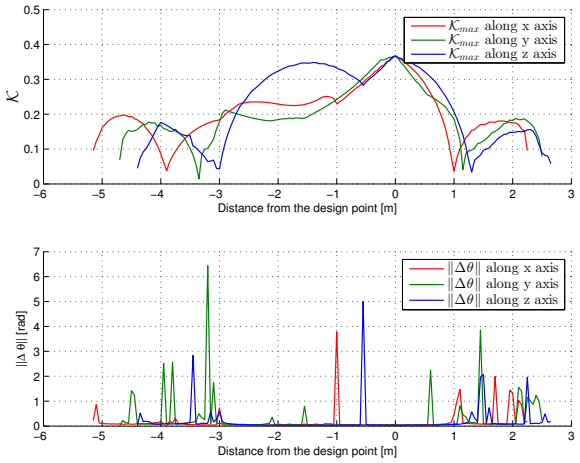

Fig. 4: The maximum value of $\mathcal{K}$ (top) and change in configuration (bottom) for trajectories along the x-axis, y-axis, and z-axis that cross the design point. This maximum value may result jumps between self-motion manifolds which are indicated by large changes in configuration.

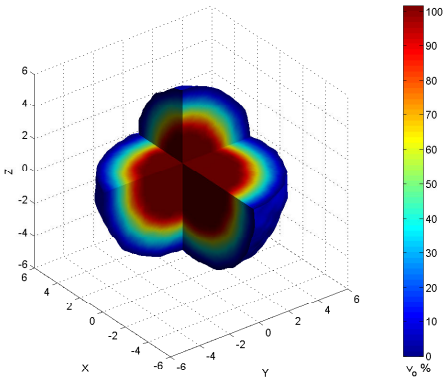

Fig. 5: Six-dimensional reachable volume. This is very similar to the fault tolerant volume for $\mathcal{K} \neq 0$. The orientation volume is represented by its color within the three-dimensional volume as a percentage of $V_{o_{max}} = \pi^2$.

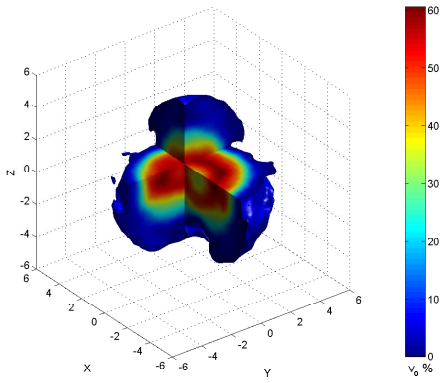

Fig. 6: Six-dimensional fault tolerant volume for $\mathcal{K} > 0.2$ that allows jumps between self-motion manifolds, which is appropriate for point-to-point tasks. The orientation volume is represented by its color within the three-dimensional volume as a percentage of $V_{o_{max}} = \pi^2$.

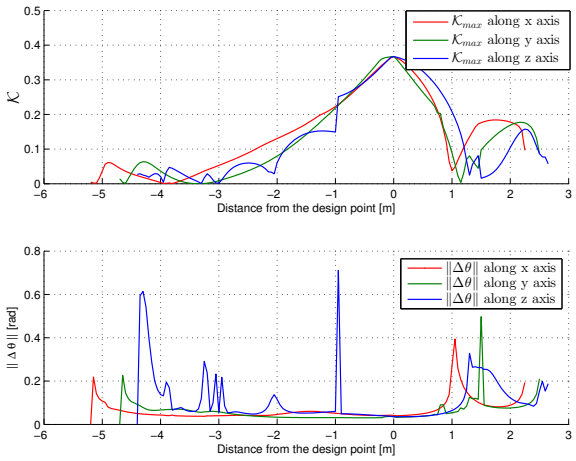

Fig. 7: The maximum value of $\mathcal{K}$ (top) and change in configuration (bottom) for trajectories along the x-axis, y-axis, and z-axis that cross the design point. This maximum value is restricted to lie in the current self-motion manifold due optimization using the projection of $\nabla\mathcal{K}$ onto the nullspace.

volume where the orientation volume is represented by its percentage of the maximum value π^2. The three-dimensional fault tolerant volume is 78% of the maximum, which defines the spatial positioning task space that is fault tolerant, whereas the six-dimensional workspace is 10% of the maximum. Fig. 6 illustrates the six-dimensional fault tolerant volume. One can see how the largest values of fault tolerant orientation volume are concentrated around the design point. Figs. 5 and 6 each took approximately ten hours to compute on the Colorado State University Cray XT6m computer.

C. Fault Tolerant Trajectories

If one is interested in the end effector following a specified trajectory, one can use the $\nabla\mathcal{K}$ projection onto the current nullspace method. This will make the robot track the maximum $\mathcal{K}$ locally on one self-motion manifold. In this example, the robot is moved from the design point to every position along the trajectory. Fig. 7 illustrates x-axis, y-axis, and z-axis trajectories when using $\nabla\mathcal{K}$. Comparing to Fig. 4, one can see how the magnitude of joint change is significantly smaller along the trajectory, which makes these trajectories feasible to use, for example, for an arc welding application. The three-dimensional fault tolerant volume in this case is 63% of the total sphere, whereas the six-dimensional workspace is 1.3% of the maximum. Table IV compares these values versus the case of fault tolerant point-to-point motion. Fig 8 illustrates the six-dimensional fault tolerant workspace, which is relatively small compared to the workspace in Fig. 6.

V. Conclusions

This work focused on the analysis of anthropomorphic manipulators, such as the PA-10, which are known to be

TABLE IV: Comparison between $\mathcal{K}$ maximization techniques

Global measure	null motion	$\nabla\mathcal{K}$
$V_{FT_{3d}}$ [%]	78	63
V_{FT} [%]	10	1.3

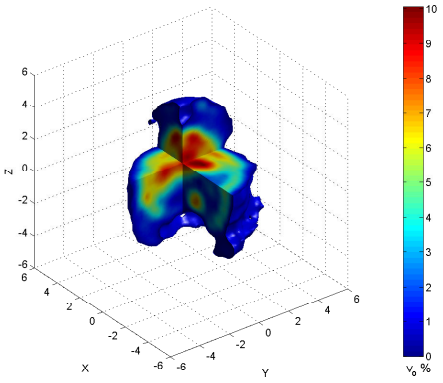

Fig. 8: Six-dimensional fault tolerant volume for $\mathcal{K} > 0.2$ that is optimized using the projection of $\nabla\mathcal{K}$ onto the nullspace, which is appropriate for following specified end-effector trajectories. The orientation volume is represented by its color within the three-dimensional volume as a percentage of $V_{o_{max}} = \pi^2$.

intolerant to a single locked joint failure. It was shown that these arms can be made significantly more fault tolerant to joint failures by a minor modification to the kinematic structure of the arm. The DH parameters for the modified arm are designed so that the corresponding fault tolerant properties are close to those of a robot with an optimally failure tolerant Jacobian. The fault tolerance of the designed robot was evaluated for two different classes of applications, i.e., point-to-point motions and specified end-effector trajectories. The technique presented here focused on optimizing a kinematic are design that was close to the of a human, i.e., PA-10. However the technique is fully general and can be applied to an arbitrary arm design.

REFERENCES

[1] S. Kawatsuma, M. Fukushima, and T. Okada, "Emergency response by robots to Fukushima-daiichi accident: Summary and lessons learned," *Industrial Robot: An International Journal*, vol. 39, no. 5, pp. 428–435, 2012.

[2] K. Nagatani, S. Kiribayashi, Y. Okada, K. Otake, K. Yoshida, S. Tadokoro, T. Nishimura, T. Yoshida, E. Koyanagi, M. Fukushima, and S. Kawatsuma, "Emergency response to the nuclear accident at the Fukushima daiichi nuclear power plants using mobile rescue robots," *Journal of Field Robotics*, vol. 30, no. 1, pp. 44–63, 2013.

[3] K. N. Groom, A. A. Maciejewski, and V. Balakrishnan, "Real-time failure-tolerant control of kinematically redundant manipulators," *IEEE Trans. Robot. Automat.*, vol. 15, no. 6, pp. 1109–1116, Dec. 1999.

[4] Reliability Information Analysis Center, "Nonelectronic parts reliability data," Defense Technical Information Center / Air Force Research Lab, Rome, NY, USA, no. NPRD-2011, 2011.

[5] P. Nieminen, S. Esque, A. Muhammad, J. Mattila, J. Väyrynen, M. Siuko, and M. Vilenius, "Water hydraulic manipulator for fail safe and fault tolerant remote handling operations at ITER," *Fusion Engineering and Design*, vol. 84, no. 7, pp. 1420–1424, 2009.

[6] S. Cheng and B. S. Dhillon, "Reliability and availability analysis of a robot-safety system," *Journal of Quality in Maintenance Engineering*, vol. 17, no. 2, pp. 203–232, 2011.

[7] L. Capisani, A. Ferrara, A. F. de Loza, and L. Fridman, "Manipulator fault diagnosis via higher order sliding-mode observers," *IEEE Transactions on Industrial Electronics*, vol. 59, no. 10, pp. 3979–3986, 2012.

[8] M. Ji and N. Sarkar, "Supervisory fault adaptive control of a mobile robot and its application in sensor-fault accommodation," *IEEE Trans. Robotics*, vol. 23, no. 1, pp. 174–178, Feb. 2007.

[9] A. De Luca and L. Ferrajoli, "A modified Newton-Euler method for dynamic computations in robot fault detection and control," in *IEEE Int. Conf. Robot. Automat.*, May 2009, pp. 3359–3364.

[10] L. Notash, "A methodology for actuator failure recovery in parallel manipulators," *Mech. Mach. Theory*, vol. 46, no. 4, pp. 454–465, 2011.

[11] A. Allais, J. McInroy, and J. O'Brien, "Locally decoupled micromanipulation using an even number of parallel force actuators," *IEEE Trans. Robotics*, vol. 28, no. 6, pp. 1323–1334, 2012.

[12] R. G. Roberts, H. G. Yu, and A. A. Maciejewski, "Fundamental limitations on designing optimally failure-tolerant kinematically redundant manipulators," *IEEE Trans. Robotics*, vol. 24, no. 5, pp. 1124–1237, Oct. 2008.

[13] R. C. Hoover, R. G. Roberts, A. A. Maciejewski, P. S. Naik, and K. M. Ben-Gharbia, "Designing a Failure-Tolerant Workspace for Kinematically Redundant Robots," accepted to appear in *IEEE Trans. Autom. Sci. Eng.*, 2015.

[14] K. M. Ben-Gharbia, A. A. Maciejewski, and R. G. Roberts, "A kinematic analysis and evaluation of planar robots designed from optimally fault-tolerant Jacobians," *IEEE Trans. Robotics*, vol. 30, no. 2, pp. 516–524, 2014.

[15] K. M. Ben-Gharbia, A. A. Maciejewski, and R. G. Roberts, "Kinematic design of redundant robotic manipulators for spatial positioning that are optimally fault tolerant," *IEEE Trans. Robotics*, vol. 29, no. 5, pp. 1300–1307, 2013.

[16] J. D. English and A. A. Maciejewski, "Fault tolerance for kinematically redundant manipulators: Anticipating free-swinging joint failures," *IEEE Trans. Robot. Automat.*, vol. 14, no. 4, pp. 566–575, Aug. 1998.

[17] P. I. Corke, "A robotics toolbox for MATLAB," *IEEE Robot. Autom. Mag.*, vol. 3, no. 1, pp. 2–32, Mar. 1996.

[18] J. Y. S. Luh, M. W. Walker, R. P. C. Paul, "Resolved-acceleration control of mechanical manipulators," *IEEE Trans. Automat. Control*, vol. 25, no. 3, pp. 468–474, Jun 1980.

[19] K. M. Ben-Gharbia, A. A. Maciejewski, and R. G. Roberts, "An example of a seven joint manipulator optimized for kinematic fault tolerance," *IEEE Int. Conf. on Syst., Man, Cybern.*, Diego, CA, Oct. 5-8, 2014, pp. 802–807.